Efficient Optimization Design of Large Circular Phased Arrays With Low Sidelobes for Beam Scanning

YI-XUAN ZHANG [1,2] (Member, IEEE), TIAN-YE GAO [2], LI ZHANG [1,2],
YONG-CHANG JIAO [2] (Senior Member, IEEE), AND TAO NI [3]

[1]Hangzhou Institute of Technology, Xidian University, Hangzhou 311231, Zhejiang, China

[2]National Key Laboratory of Antennas and Microwave Technology, Xidian University, Xi'an 710071, Shaanxi, China

[3]The 20th Institute of Chinese Electronics Technology Company, Xi'an 710068, China

CORRESPONDING AUTHOR: L. ZHANG (e-mail: lizhang@mail.xidian.edu.cn)

ABSTRACT This paper proposes an efficient optimization design method for large circular phased arrays with low sidelobes for beam scanning. Based on the differential evolution algorithm (DE), each layer's radius and element number are optimized to obtain the required element arrangement. If the main beam scans from the Z-axis, it is difficult for designers to find the maximum sidelobe. In addition, a computer with a large memory is required to achieve the final fine verification of the array elements arrangement, and the calculation time is unbearable. To solve these problems, the array structure is rotated so that the direction of the main beam is rotated to the Z-axis, and then the radiation pattern is divided into high-density and low-density areas for random sampling, which improves the calculation speed while ensuring the calculation accuracy. To quickly verify whether the array arrangement obtained by the final design meets the performance requirements, the radiation pattern of the final result is distributed to multiple computers for distributed calculation, which significantly reduces computer memory and time consumption. The numerical experiment shows that the method proposed in this paper can obtain the array arrangement that meets the performance requirements in a short optimization time.

INDEX TERMS Large circular array, phased array, beam scanning, low sidelobe, differential evolution algorithm (DE).

I. INTRODUCTION

IN RADAR detection, to obtain a long detection range and high angular resolution, high antenna gain and low radiation pattern sidelobes are required in the antenna system [1]. A single antenna usually cannot meet the performance requirements, and combining antennas into an array can significantly increase the overall gain and reduce the maximum sidelobe. A circular array is a common form of the planar array [2], [3], [4], [5], [6], [7], [8], [9], it is often used in radar tracking, remote sensing, biomedical imaging, satellites, ground communication, and other applications

[10], [11], [12]. The circular array is geometrically symmetric with respect to the center of the circular ring, so the circular array can provide a nearly constant beam pattern for 360° azimuth coverage [5], [13], [14], [15]. The circular array can consist of either a single ring [16], [17], [18], [19] or multiple concentric rings [20], [21], [22], [23]. The gain of the array is mainly determined by the size of aperture. For circular arrays, designers can obtain higher gains by setting more ring layers. There are mainly two ways to achieve low sidelobe for circular arrays. The first is to adjust the amplitude of the feed in each element, and the second

is to adjust the distance between the elements [24], [25]. Although the second way for sidelobe reduction is not manifest as the first one, it can ensure that the power of each element is not lost, so the second way is chosen to achieve low sidelobe performance in this work. Besides, the array needs to have a certain scanning angle to realize the detection function within a given space coverage. Compared with the mechanical scanning method of rotating the array arrangement, controlling each element's feeding phase to realize beam scanning is faster and more reliable [26], [27].

Determining the location of elements in a phased array is a difficult and time-consuming task. The optimization of the element position of circular arrays is temporarily difficult to be converted into convex optimization, so efficient and robust convex optimization may not be effectively introduced. Designers often use global optimization algorithms to determine the element position of circular arrays [28], [29]. Differential evolution algorithm (DE) is an efficient global optimization algorithm [30], which is often used for the optimal design of antenna structure parameters and array element arrangement because of its simplicity and robustness [31], [32], [33], [34]. In this work, DE is used to optimize each layer's radius and element number, which can used to calculate the position of each element, so that the array can meet the requirements of the sidelobe in all scanning angles.

When DE is used for optimization, the fitness function is the main factor we need to consider first. To minimize the maximum sidelobe, we first need to express the maximum sidelobe of the radiation pattern in a mathematical form. However, once the direction of the main beam scans from the Z-axis, it is difficult to accurately and quickly find the maximum sidelobe from the main beam to the surroundings. In addition, after finding a satisfying solution using DE, designers need to verify whether it meets the performance requirements. It is usually necessary to finely sample and calculate the 3D radiation pattern. The sampling points are dense, so a large amount of data needs to be stored. Therefore, a large computer memory is required and the calculation time may also be unbearable.

In order to solve these problems, three innovations are proposed in this paper to accurately and quickly find the maximum sidelobe of the radiation pattern, and significantly reduce the time consumption of the final fine verification. Firstly, to numerically find the maximum sidelobe from the main beam to the surroundings, the array structure is rotated so that the main beam turns to the Z-axis. At this time, designers only need to find the maximum sidelobe on each φ cut-plane of the radiation pattern, which simplifies the process of finding the maximum sidelobe. Secondly, when looking for the sidelobe of the radiation pattern, the calculation speed and the accuracy of the founded sidelobe are two conflicting parts. To improve the calculation speed under the premise of adequate sidelobe accuracy, a random sampling method with unequal density is proposed. To prevent the

largest sidelobe from being missed, high-density fine sampling is performed in areas where the main lobe is likely to exist. Low-density coarse random sampling is performed in other areas to improve calculation speed. The sampling point locations are changed randomly with each DE iteration, to prevent the final result from meeting performance requirements only at fixed sampling points. Lastly, to reduce the memory requirement of a single computer and calculation time consumption in the final fine verification, each φ cut-plane of the radiation pattern is assigned to different computers for parallel distributed computation. Because the computation is distributed across multiple computers, the memory consumption for each computer is reduced. Thanks to the parallel calculation method, the calculation time is greatly shortened. Distributed radiation pattern computing significantly reduces the memory requirements of the computer, improves the verification speed, and also makes it possible to implement fine verification in personal computers.

Numerical experiments are used to verify the effectiveness of the proposed method. The rest of this paper is arranged as follows. **Section II** introduces the arrangement of the circular array elements. **Section III** introduces the optimization design process of this method. In **Section IV**, the method is used in numerical experiments to prove its effectiveness. In **Section V** concluding observations are given.

II. ARRAY BASIC THEORY AND ARRANGEMENT OF CIRCULAR ARRAY ELEMENTS

Consider a N-element antenna array with the nth element R_n located at $(x_n, y_n, 0)$ in the Cartesian coordinate system. For an observing at direction (θ, φ), where θ and φ are the angular in the global spherical coordinate system, the far-field pattern $F(\theta, \varphi)$ can be expressed by

$$F(\theta, \varphi) = \sum_{n=1}^{N} f_n^{ele}(\theta, \varphi) w_n e^{jk(x_n \sin\theta \cos\varphi + y_n \sin\theta \sin\varphi)} \quad (1)$$

where $f_n^{ele}(\theta, \varphi)$ is the radiation pattern of each element, w_n is the complex excitation of the nth element. If all antenna elements in the array have the same element pattern and ignoring the differences in each element pattern caused by mutual coupling effects, $f_n^{ele}(\theta, \varphi)$ can be replaced by $f^{ele}(\theta, \varphi)$. Then Equation (1) can be further expressed as

$$F(\theta, \varphi) = f^{ele}(\theta, \varphi) \sum_{n=1}^{N} w_n e^{jk(x_n \sin\theta \cos\varphi + y_n \sin\theta \sin\varphi)}$$
$$= f^{ele}(\theta, \varphi) f(\theta, \varphi) \quad (2)$$

where $f^{ele}(\theta, \varphi)$ is the pattern of the same array element, $f(\theta, \varphi)$ is the array factor. Equation (2) is also known as the pattern multiplication theorem, which is used to calculate the array pattern.

As an important indicator of the array, the sidelobe can reflect the concentration of energy. Before finding the maximum sidelobe, it is necessary to find the first nulls, which
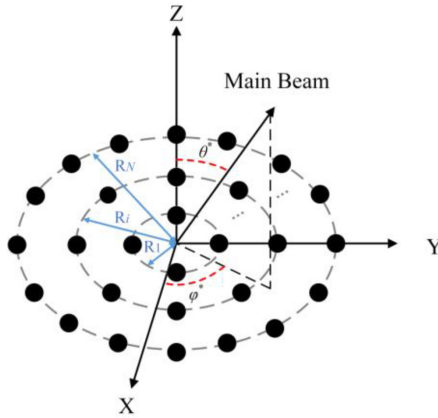
FIGURE 1. Original array element arrangement.

is the first minimum value found on the side from the maximum radiation direction. The first nulls divide the pattern into the sidelobe region and the main lobe region. The maximum sidelobe is the maximum value in the sidelobe region. Gain is another important performance indicator of the array. The larger gain allows signals to be transmitted further. The gain can be calculated as follows

$$G(\theta, \varphi) = \eta \frac{4\pi |F(\theta, \varphi)|^2}{\int_0^{2\pi} \int_0^{\pi} |F(\theta, \varphi)|^2 \sin\theta d\theta d\varphi} \quad (3)$$

where η is the radiation efficiency. For the phased array, designers mostly try to maximize the gain in the desired main beam direction.

In this research, the main beam angle of the beam scanning array can be described by θ^* and φ^*, where θ^* represents the angle between the main beam direction and the Z-axis, and φ^* represents the angle between the main beam direction and the *xoz* plane. As a strongly symmetrical array composition method, the circular array has the characteristic that the element arrangement is still approximately the same after rotating at any angle with the z-axis as the rotation axis, so the scanning angle in the φ direction has minor influence on the difference of maximum sidelobe level.

The arrangement of the array elements is shown in Fig. 1, and each black circle in the figure represents an antenna element. The entire array is composed of N layers of circular rings, and the radius of each circular ring is R_i, $i=1, 2, \ldots, N$. Any two adjacent elements of this circular array on each layer of the circular ring have the same angle difference, so adjusting the radius R_i of the circular ring and the number of elements M_i of each circular ring can effectively adjust the distance between the elements.

III. THE PROCESS OF OPTIMAL DESIGN
A. PROBLEMS AND DIFFICULTIES
For large arrays, designers often need to find the maximum sidelobes in each φ cut-plane of the radiation pattern. As shown in Fig. 2, the main beam direction scans from the Z-axis due to beam scanning. In this case, designers cannot tell whether the maximum in each φ cut-plane is the
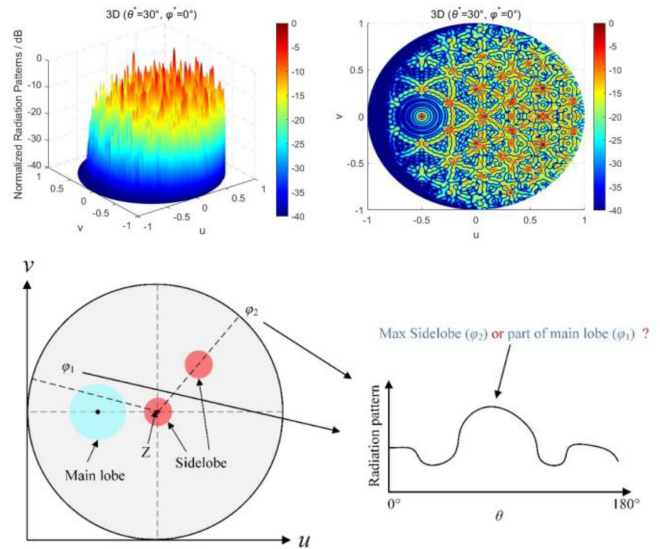

FIGURE 2. The process of finding sidelobes.

true maximum sidelobe or part of the main lobe. Therefore, the process of finding sidelobes cannot be easily realized. In addition, because designers cannot determine where sidelobes may exist, global high-density sampling of the radiation pattern is required. This consumes a lot of computer memory and computing time, which is obviously unbearable for population-based algorithms that need to repeatedly calculate radiation patterns.

For a large circular array with 10 rings, let's assume that the main beam is not scanned, and its main beam points to the Z-axis. The angle needs to be calculated is $\theta \in [0, 90^\circ]$ $\cup \varphi \in [0, 360^\circ]$. To sample the entire array radiation pattern globally with equal density at a sampling interval of 0.05°, the amount of sampling point data that needs to be stored is 1800×7200, which is about 1.3×10^7. The radiation patterns of all antenna elements need to be considered at each sampling point. Assuming that there are 2500 antenna elements in total, the amount of data that needs to be stored in the computer memory during the calculation is 3.24×10^{10}. Ordinary personal computers are usually unable to store such massive amounts of data during calculations. Even if the calculation can be done, the time-consumption is prohibitive. When verifying the final arrangement of array elements, the same large number of sampling points also need to be calculated. Therefore, it is difficult to optimize large circular arrays for designers using existing methods.

B. ALGORITHMIC FRAMEWORK
Phased arrays usually need to achieve the required performance indicators within a certain scanning angle. Thanks to the nearly symmetrical arrangement of the circular array, the pattern difference in the beam scanning angles with different φ direction is almost negligible, thus we mainly consider the down-tilt angle θ^* of the beam scanning. Through a lot of experiments, we have observed that for the

same array arrangement, the sidelobe and gain obtained at the maximum down-tilt angle $\theta^*_{\max}$ of the main beam are the worst values within the beam scanning range. Therefore, as long as the performance at the maximum down-tilt angle $\theta^*_{\max}$ can achieve the optimization target, other scanning angles are also able to meet the design requirements. In this work, only the maximum sidelobe in the main beam direction $(\theta^*_{\max}, 0^\circ)$ is optimized. After the arrangement of the array elements is obtained, the multiple scanning angles are verified to ensure that design specifications are met. The results confirm that only optimizing the array elements arrangement in $(\theta^*_{\max}, 0^\circ)$ direction scanning case can sufficiently get the results that meet the design requirements.

The design goal of the circular array is to meet the sidelobe and gain requirements within a given main beam scanning range. The gain depends on the aperture size of the array, and a sufficient number of circular layers can be selected to meet the gain index. In this work, the radius and the number of elements of each circular ring are mainly optimized to achieve as low a sidelobe as possible. The fitness function F can be expressed by the following equation

$$F = \max_{\varphi_i \in [\varphi_1,\ldots,\varphi_n]} 20 \cdot \lg \left| \frac{AF_{\text{side},\theta^*_{\max}}(\varphi_i)}{AF_{\text{main},\theta^*_{\max}}} \right| \qquad (4)$$

In Equation (4), $\theta^*_{\max}$ represents the maximum down-tilt angle of the main beam scan. $\varphi_1 \sim \varphi_n$ divide the radiation pattern into n cut-planes, and i represents the index of the φ cut-plane. $AF_{\text{main},\theta^*_{\max}}$ represents the maximum main lobe of the radiation pattern at the maximum down-tilt angle, and $AF_{\text{side},\theta^*_{\max}}(\varphi_i)$ represents the maximum sidelobe of the φ_i cut-plane radiation pattern at the maximum down-tilt angle.

How to accurately and quickly find $AF_{\text{side},\theta^*_{\max}}(\varphi_i)$ is the main difficulty in optimizing the maximum sidelobe of the phased array with scanned main beam. As mentioned in **Section I**, this work proposes measures such as rotating array structure, unequal-density random sampling, and distributed computing for radiation patterns, which greatly accelerates the calculation speed and reduces the optimization time under the premise of ensuring the accuracy of obtained sidelobes.

The specific operation of this method is shown in Fig. 3. Firstly, the initial parent population is randomly generated and the fitness value of each individual is calculated. Then the mutation and crossover operation of DE is executed to generate an offspring population. Afterward, the fitness function of each offspring individual is calculated, and the selection operation is executed in which individuals with lower fitness values are retained to form a new population. Finally, it is judged whether the stop criterion is satisfied. If yes, the distributed calculation of the precise radiation pattern is executed. Otherwise, the mutation and crossover operation will be re-executed to generate a new offspring population. When calculating the fitness, the array structure is firstly rotated so that the main beam points to the Z-axis, and then the radiation pattern is unequal-density random sampled. Afterward, the maximum sidelobe in each φ cut-plane
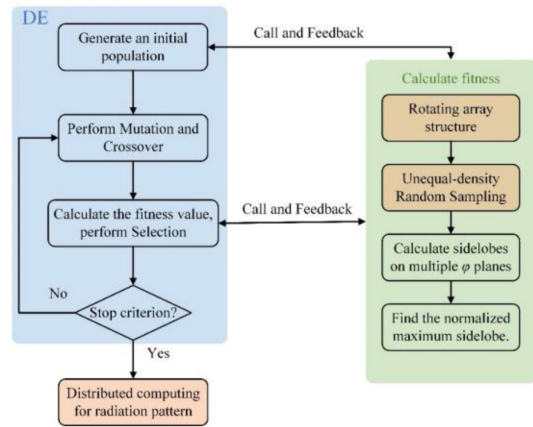

FIGURE 3. The process of the proposed optimization design method.
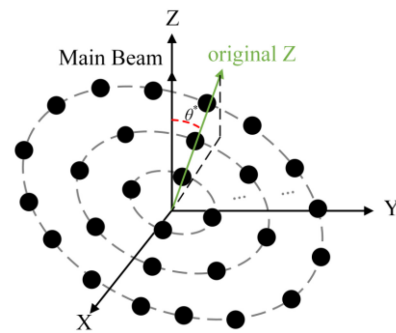

FIGURE 4. Array element arrangement after rotating the array structure.

is calculated. Finally, the fitness value which represents the normalized maximum sidelobe is obtained by Equation (4).

The measures of rotating array structure, unequal-density random sampling, and distributed calculation of radiation patterns will be described in detail in Sections III-C~III-E.

C. ROTATING ARRAY STRUCTURE

Finding the maximum sidelobe is essentially a peak-finding problem, which is finding a second peak beside the maximum peak. When the main beam scans from the Z-axis, due to the limitations of the spherical coordinate system, it is difficult to accurately realize the process of finding the second peak from the maximum peak to its surroundings. In this case, as Fig. 4 shows, we rotate the position coordinates of each element in the array to translate the main beam direction to the Z-axis. The process of rotating the array structure can be described as follows

$$\begin{pmatrix} X \\ Y \\ Z \end{pmatrix} = T_1 \cdot \left(T_2 \cdot \begin{pmatrix} X^* \\ Y^* \\ Z^* \end{pmatrix} \right) \qquad (5)$$

$$T_1 = \begin{bmatrix} \cos\theta^* & 0 & -\sin\theta^* \\ 0 & 1 & 0 \\ \sin\theta^* & 0 & \cos\theta^* \end{bmatrix} T_2 = \begin{bmatrix} \cos\varphi^* & \sin\varphi^* & 0 \\ -\sin\varphi^* & \cos\varphi^* & 0 \\ 0 & 0 & 1 \end{bmatrix} \qquad (6)$$

In Equation (5), X, Y, and Z are the new position coordinates of each element obtained after rotating the array
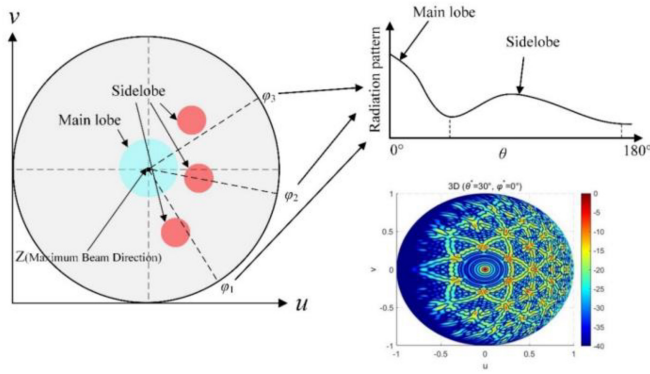
FIGURE 5. The process of finding sidelobes after rotating the array structure.

FIGURE 6. Schematic diagram of the unequal-density random sampling.

structure. Whereas X^*, Y^*, and Z^* are the original space coordinates of each element. In Equation (6), operator T_2 rotates each element around the Z-axis in order to rotate the main beam pointing to the *xoy* plane. Operator T_1 rotates the array coordinates obtained by T_2 with the Y-axis as the rotating axis and finally obtaining the main beam pointing to the Z-axis.

As shown in Fig. 5, after rotating the array structure, the main beam accurately points to the Z-axis. When looking for the maximum sidelobe in each φ cut-plane, $\theta=0°$ direction is the maximum beam direction. At this point, we can ensure that the second peak is the sidelobe of this φ cut-plane. After all φ cut-planes are calculated, the maximum sidelobe obtained in all φ cut-planes is the maximum sidelobe in the whole radiation pattern. This method greatly simplifies the process of finding the maximum sidelobe and establishes the foundation for the subsequent unequal-density random sampling.

D. UNEQUAL-DENSITY RANDOM SAMPLING

As shown in Equation (4), the main lobe and the maximum sidelobe need to be found exactly to calculate the fitness value. After the array structure is rotated, the main lobe $AF_{\mathrm{main},\theta^*_{\max}}$ can be easily found in $\theta=0°$ direction. At this time, we only need to find the maximum sidelobe of the radiation pattern in each φ cut-plane. The accuracy of finding the maximum sidelobe is directly related to the density of sampling points. In order to avoid that missing directions do not meet the sidelobe requirements, the radiation pattern is usually finely sampled, but this unbearably consumes a lot of computer resources due to large computational time consuming.

In order to achieve the optimization goal faster on the premise of ensuring the calculation accuracy of the sidelobe, we propose an unequal-density random sampling method. A real 3D radiation pattern is shown in Fig. 6(A) and Fig. 6(B). As can be seen in the figure, after rotating the array structure, the main beam points to the Z-axis, whereas the original Z-axis has a certain down-tilt. The area around the original Z-axis and the main beam is more likely to have the maximum sidelobe, which is marked as blue area
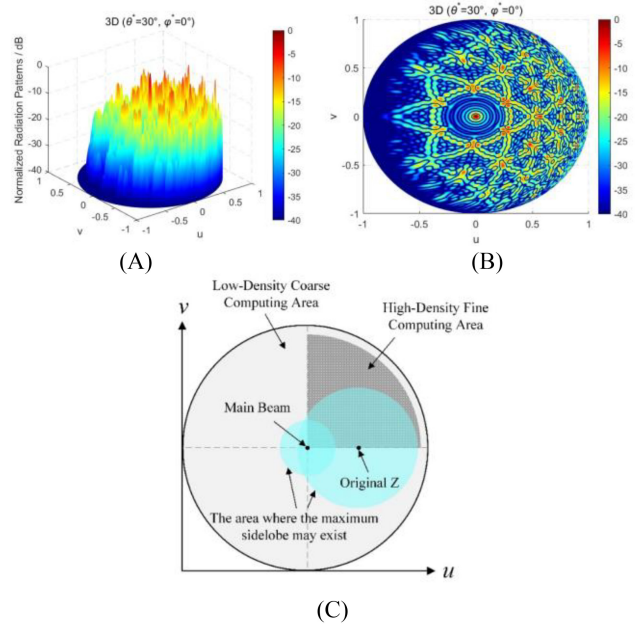
in Fig. 6(C). Therefore, we divide the high-density computing area and the low-density computing area as shown in the dark gray area in Fig. 6(C). High-density fine calculation of this area can avoid missing the maximum sidelobe.

Since the arrangement of the circular array elements is near-axisymmetric, we only need to set the fine calculation area to cover all half of the blue area to ensure that the maximum side lobe is not missed. In this work, we set the maximum down-tilt angle of the beam to be $\theta^*_{\max}$. After rotating the array structure, the main beam points to the Z-axis, and the original Z-axis down-tilt angle is also $\theta^*_{\max}$. We take the original Z-axis downward direction as the reference $0°$ direction of φ, and sample the radiation pattern with a high density in the area of $\varphi \in [0°, 90°] \cup \theta \in [0°, \theta^*_{\max}+20°]$. In the rest of the area, only low-density sampling is performed, which realizes the unequal-density setting of sampling points, and improves the optimization speed on the premise of ensuring the accuracy of sidelobe estimation.

DE is a "greedy" and "cunning" global optimization algorithm. In order to find the arrangement corresponding to the lower fitness function, the maximum sidelobe may shift toward the area where no sampling points are set as the optimization proceeds. At this time, although the normalized maximum sidelobe value obtained by the optimization result meets the design target, the real maximum sidelobe may not fully satisfy the needs after precise calculation. To solve this problem, we set a random perturbation at each sampling point. The calculation process of the sampling point coordinates position is shown as follows

$$\theta_{i,j} = \Delta\theta \cdot \left(i-1+\alpha \cdot r_{i,j}\right) \qquad \varphi_{i,j} = \Delta\varphi \cdot \left(j-1+\alpha \cdot r_{i,j}\right)$$

$$(7)$$

TABLE 1. Comparison of two radiation pattern calculation methods.

	Time (S)	Time comparison (%)	Results (dB)	Accuracy (%)
Unequal-density Random Sampling	67	22.3	-22.01	97.8
Global high-density sampling	300	100	-21.54	100

where i represents the index number of the sampling point in the θ direction, j represents the index number in the φ direction, $\Delta\theta$ represents the sampling interval in the θ direction, and $\Delta\varphi$ represents the sampling interval in the φ direction. Besides, r represents a random number generated according to the standard normal distribution probability. According to the 3σ principle, in order to make the upper and lower limits of the disturbance variation both range 0.5 times the sampling interval, α is set to 0.16.

The position of each sampling point is not fixed but changes randomly with the optimization, thus preventing the final optimization result from meeting the sidelobe requirement only at the fixed sampling point. The problem of excessive deviation between the optimization result and the final fine calculation result has been effectively solved.

In order to distinguish between unequal-density random sampling and global high-density sampling, a numerical experiment is performed. We use these two methods to calculate an existing 20-layer circular array, and the calculation results are shown in Table 1. The unequal-density sampling method proposed in this paper achieves an accuracy rate of 97.8% in only 22.3% of the calculation time of high-density sampling, which significantly shortens the calculation time while ensuring high calculation accuracy. In addition, as shown in Fig. 6(C), due to the significant reduction in the number of sampling points (only less than 25% of the original), the consumption of computer memory is also greatly reduced. This method makes the optimization of large circular arrays possible for individual designers.

E. DISTRIBUTED COMPUTING FOR RADIATION PATTERNS

For the final arrangement of array elements, we need to verify whether the design specifications are met. The common method is to sample at high density in all directions and calculate the value of each sampling point. As the sampling density in the θ and φ directions increases, the number of sampling points also increases quadratically, and personal computers usually cannot store such a large amount of data. Because the amount of data to be calculated is so large, even for a server host with sufficient computer memory, the calculation time is also unbearable.

In order to solve the above problems, we introduce a distributed computing method for radiation patterns. As shown in Fig. 7, the radiation pattern is divided into multiple φ cut-planes at a fixed angular interval $\Delta\varphi$, and each φ cut-plane is assigned to different computers for distributed computing. Each computer only calculates several φ cut-planes and
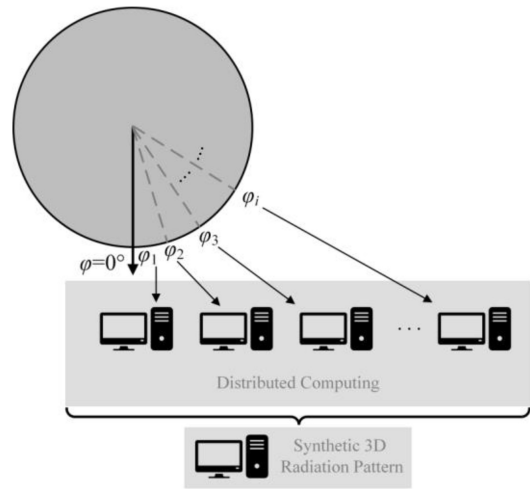

FIGURE 7. Schematic diagram of distributed computing for radiation patterns.

saves the calculation results in external files. After the calculation of all φ cut-planes is completed, we aggregate all calculated external files to synthesize the final 3D radiation pattern. The distributed computing operation of the radiation pattern not only reduces the memory consumption of a single computer but also greatly shortens the computing time.

For the calculation examples given in Section III-A, we use distributed computing for radiation patterns to illustrate the advantages of this method. Since the sampling interval is $0.05°$, a total of 7200 φ cut-planes need to be calculated. Then we assign several φ cut-plane to a different computer; thus, the computational complexity of a single computer is reduced. During the calculation process, the amount of data that each computer needs to store and calculate has dropped greatly, which reducing the memory consumption of a single computer. Furthermore, since the computation is distributed across multiple computers, each computer only needs to compute small portion of the original data. Therefore, thanks to the parallel calculation method, the calculation time consumption is significantly reduced.

IV. NUMERICAL EXPERIMENTS

The experiment was performed in computers with Intel 13700K processor and MATLAB R2022. In order to verify the effectiveness of the proposed method, we use this method to design a large circular phased array to meet the target requirements. The design goal is to realize the arrangement of array elements operating at a band of $0.9f \sim 1.1f$, with f the center frequency. The gain is greater than 40 dBi within the beam scanning range of $\theta^* \in [0, 30°]$, $\varphi^* \in [0, 360°]$, and the maximum sidelobe of the radiation pattern is less than -20 dB and be reduced as much as possible.

In order to meet the sidelobe requirements without reducing the power radiation of the elements, we need to optimize the distance between the elements. The variables to be optimized are the radius of each circular and the
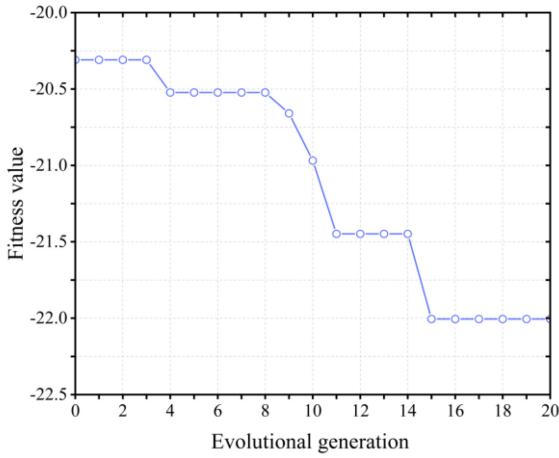
FIGURE 8. Optimizing process for array element locations.

FIGURE 9. The resulting arrangement of the optimized array elements (λ is the wavelength in the center frequency f).

TABLE 2. Each layer's radius and element number obtained by optimization.

layer	1	2	3	4	5	6	7
Radius (λ)	35.4	72.7	110	126	154	180	215
Number	12	60	60	186	378	354	60
layer	8	9	10	11	12	13	14
Radius (λ)	248	274	298	318	349	374	399
Number	144	306	786	78	546	138	234
layer	15	16	17	18	19	20	
Radius (λ)	409	420	432	459	491	512	
Number	270	804	192	162	750	126	

TABLE 3. Maximum sidelobe and gain of the final array arrangement corresponding to different main beam scanning angles in 0.9f, 1f and 1.1f frequencies.

0.9f	$(0°, 0°)$	$(10°, 30°)$	$(20°, 45°)$	$(30°, 90°)$
Sidelobe (dB)	-22.92	-22.95	-22.15	-21.54
Gain (dBi)	43.51	43.38	42.97	42.26
f	$(0°, 0°)$	$(10°, 30°)$	$(20°, 45°)$	$(30°, 90°)$
Sidelobe (dB)	-23.37	-22.71	-22.48	-21.72
Gain (dBi)	43.5	43.38	42.97	42.26
1.1f	$(0°, 0°)$	$(10°, 30°)$	$(20°, 45°)$	$(30°, 90°)$
Sidelobe (dB)	-23.45	-22.89	-22.35	-21.53
Gain (dBi)	43.52	43.38	42.97	42.26

number of elements. The radius range of each circular is $\Delta r \in [3.5\lambda, 42\lambda]$, where λ is the wavelength calculated based on the center operating frequency f. As the number of layers of the circular ring n increases, the element number of each circular ring is $M \in [6n, 72n]$.

To meet the gain specification, the array needs to contain a sufficient number of elements. The number of elements in each ring can be roughly estimated as $39n$, so the overall gain can also be estimated as

$$\text{Gain} = 10 \cdot \lg\left(\sum_{n=1}^{N} 39n\right) + \text{Gain}_{\text{single}} \qquad (8)$$

where N is the total number of layers of the circular array and Gain is the total gain of the array, $\text{Gain}_{\text{single}}$ is the gain of each element. In the numerical experiment, the element is assumed to be an ideal point source. When setting $N=20$, the estimated Gain is above 40 dBi and meets the gain requirement. Therefore, N is initially set to 20 in this numerical experiment.

The optimization convergence process is shown in Fig. 8. After 20 iterations of optimization, the fitness value is below -22. The obtained array structure is expected to meet the sidelobe requirement. The final array arrangement is shown in Fig. 9. Each blue circle in Fig. 9 represents an antenna element. The radius and the element number of each layer obtained by optimization are shown in Table 2. Finally, we calculate the optimized element arrangement to verify whether it meets the design target. Due to the near symmetry of the circular array, we only give the radiation pattern and gain performance of the four beam scanning directions $(\theta^*=0°, \varphi^*=0°)$, $(\theta^*=10°, \varphi^*=30°)$, $(\theta^*=20°, \varphi^*=45°)$ and $(\theta^*=30°, \varphi^*=90°)$ after rotating the array structure. The performance results are shown in Fig. 10, f is the center frequency desired by the designer. In order to verify the broadband performance of the final array element arrangement, we also verified the performance in the frequencies 0.9f and 1.1f. The results are shown in Fig. 11 and Fig. 12.
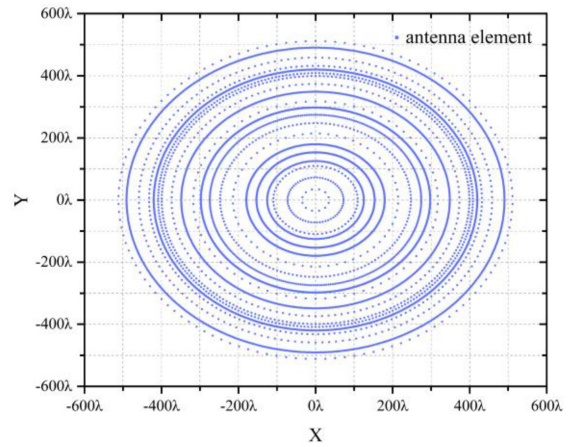
Sidelobe and gain of the final array arrangement corresponding to different main beam scanning angles in 0.9f, f and 1.1f frequencies can be seen in Table 3. In the results given in Table 3, all gains are larger than 40 dBi, and all maximum sidelobes are below -20 dB. The obtained array arrangement achieves the required performance at the given four main beam angles in f, 0.9f, and 1.1f frequencies. Therefore, we conclude that the obtained array element arrangement can meet the performance requirements in the beam scanning range in a wide frequency band covering 0.9$f \sim$1.1f frequency. If the main beam scans from the Z-axis, the existing method cannot quickly obtain the array arrangement that meets the maximum sidelobe requirement. The method proposed in this paper can obtain a satisfactory solution in a relatively short time, which proves its effectiveness.
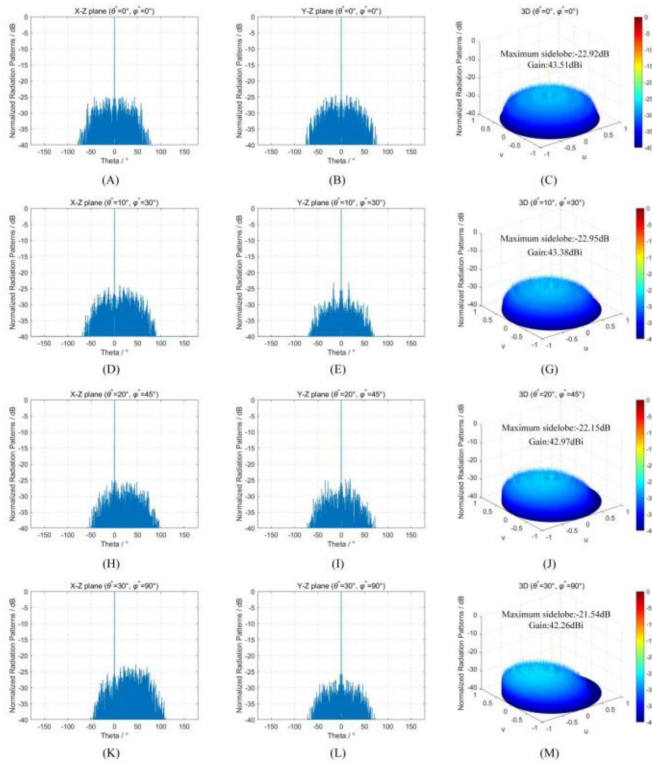
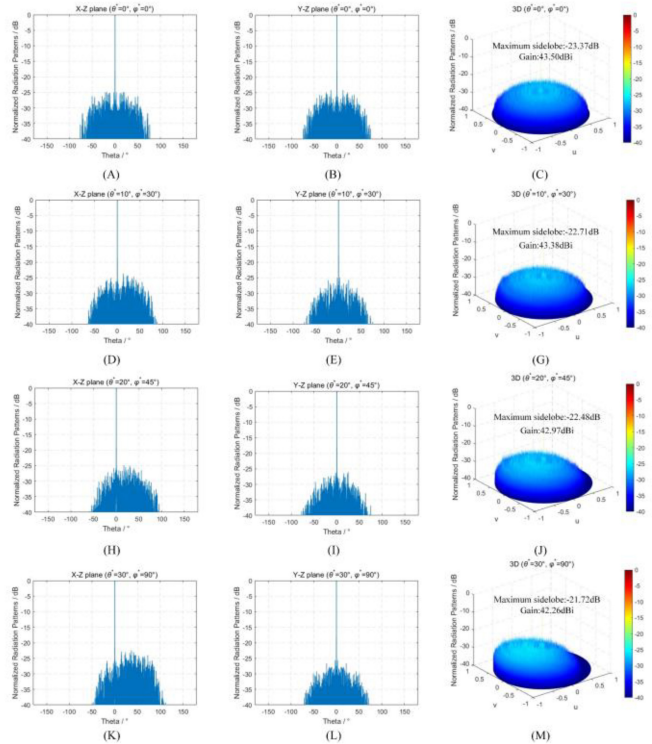FIGURE 10. Calculation results obtained by fine verification in *f* frequency.

FIGURE 12. Calculation results obtained by fine verification in 1.1*f* frequency.

FIGURE 11. Calculation results obtained by fine verification in 0.9*f* frequency.

V. CONCLUSION

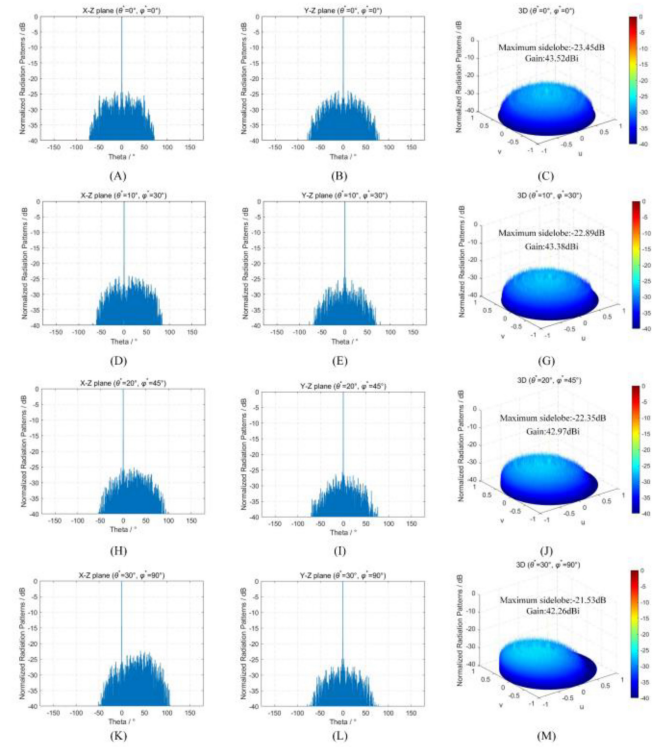The accurate and fast finding of phased array sidelobes is a difficult task. In addition, a computer with a large memory is required to achieve the final fine verification of the array elements arrangement, and the calculation time is unbearable. To solve these problems, this paper presents a method to optimize the position of the elements in the large circular phased array, which realizes the low maximum sidelobe of the radiation pattern in a short optimization time. In this method, the main beam is rotated to the Z-axis by rotating the array structure. The calculation speed is improved under the premise of ensuring the calculation accuracy through unequal-density random sampling. The final element arrangement is calculated carefully to determine whether it meets the design goals, and the operation of distributed computing for radiation patterns can assign several φ cut-planes of the radiation pattern to different computers. After all the φ cut-planes are calculated, the calculation results are summarized on a core-computer and synthesized into a 3D radiation pattern, which solves the problem of excessive computer memory requirements and unbearable time consumption. Through numerical experiments, the effectiveness of this method has been verified, and it is confirmed that this method is an effective solution for the optimal design of the element position in a large circular phased array.

VI. FUTURE WORK

As a common array optimization technique, convex optimization has significant advantages over DE in optimization efficiency. The ability to convert non-convex problems into convex problems is a prerequisite for its effectiveness. At present, in the field of circular array

optimization, convex optimization is mainly used to optimize the amplitude and phase of the element. For the element position optimization problem of a circular array that cannot be transformed into a convex problem, the designer still uses a global optimization algorithm to solve it. Inspired by [35], in the future work, we will consider the combination of convex optimization and DE to study a hybrid optimization algorithm that can simultaneously optimize the element position as well as the feeding amplitude and phase to achieve better and more flexible array performance.

APPENDIX A

The purpose of this section is to supplement the details of the circular array element position generation process. The optimization variables given in this paper are the radius and the total element number of each circular ring. Assume that the total number of elements on the i-th layer ring is M_i, and the radius is R_i. Then the polar coordinates of the j-th element on the i-th ring can be described as

$$\begin{cases} \Phi_{ij} = \frac{2\pi}{M_i - 1} j \\ P_{ij} = R_i \end{cases} \qquad (9)$$

Then convert the polar coordinates to get the Cartesian coordinates of each unit

$$\begin{cases} x_{ij} = P_{ij} \cdot \cos \Phi_{ij} \\ y_{ij} = P_{ij} \cdot \sin \Phi_{ij} \end{cases} \qquad (10)$$

Finally, the radiation pattern of the array can be obtained by calculating Equation (2).

APPENDIX B

All elements are excited uniformly, thus they have the same feeding amplitude. Each element can reach its maximum power with no power lost. The purpose of this section is to supplement how to determine the feeding phase of each element. Assuming that the required array main beam direction is in (θ, φ). Firstly, we need to calculate the projection coordinates (u_0, v_0) of the main beam on the xoy plane.

$$\begin{cases} u_0 = \sin \theta \cos \varphi \\ v_0 = \sin \theta \sin \varphi \end{cases} \qquad (11)$$

In order to use the feeding phase difference to offset the wave path difference so that the radiation of each element in (θ, φ) direction can be superimposed, the feeding phase of each element is determined by the following equation

$$pha_{ij} = -k(u_0 \cdot x_{ij} + v_0 \cdot y_{ij}) \qquad (12)$$

where k is the wave number at frequency f, which can obtained by following equation

$$k = \frac{2\pi}{\lambda} = \frac{2\pi f}{c} \qquad (13)$$

here c is the propagation speed of light, f is the frequency that the array is expected to operation, and λ is the wavelength corresponding to the operating frequency.

REFERENCES

[1] Z. J. Jiang, S. Zhao, Y. Chen, and T. J. Cui, "Beamforming optimization for time-modulated circular-aperture grid array with DE algorithm," *IEEE Antennas Wireless Propag. Lett.*, vol. 17, no. 12, pp. 2434–2438, Dec. 2018.

[2] A. Hammami, R. Ghayoula, and A. Gharsallah, "Uniform circular phased arrays synthesis using SQP algorithm," in *Proc. 11th Mediterr. Microw. Symp. (MMS)*, Yasmine Hammamet, Tunisia, 2011, pp. 185–188.

[3] G. V. Raviteja, K. Sridevi, A. Rani, and V. Rao, "Adaptive uniform circular array synthesis using cuckoo search algorithm," *J. Electromagn. Anal. Appl.*, vol. 8, no. 4, pp. 71–78, Apr. 2016.

[4] B. P. Kumar and G. R. Branner, "Generalized analytical technique for the synthesis of unequally spaced arrays with linear, planar, cylindrical or spherical geometry," *IEEE Trans. Antennas Propag.*, vol. 53, no. 2, pp. 621–634, Feb. 2005.

[5] Y. Li, K. C. Ho, and C. Kwan, "3-D array pattern synthesis with frequency invariant property for concentric ring array," *IEEE Trans. Signal Process.*, vol. 54, no. 2, pp. 780–784, Feb. 2006.

[6] R. L. Haupt, "Optimized element spacing for low sidelobe concentric ring arrays," *IEEE Trans. Antennas Propag.*, vol. 56, no. 1, pp. 266–268, Jan. 2008.

[7] A. Reyna and M. A. Panduro, "Design of steerable concentric rings array using rotation properties and evolutionary optimization," in *Proc. 4th Eur. Conf. Antennas Propag.*, Barcelona, Spain, 2010, pp. 1–5.

[8] A. Reyna, M. A. Panduro, and C. D. Rio, "Design of concentric ring antenna arrays for isoflux radiation in GEO satellites," *IEICE Electron. Expr.*, vol. 8, no. 7, pp. 484–490, 2011.

[9] A. Chatterjee, G. Mahanti, and A. Chatterjee, "Design of a fully digital controlled reconfigurable switched beam concentric ring array antenna using firefly and particle swarm optimization algorithm," *Prog. Electromagn. Res. B.*, vol. 36, pp. 113–131, Nov. 2011.

[10] L. Zhang, Y.-C. Jiao, B. Chen, and Z.-B. Weng. "Design of wideband concentric-ring arrays with three-dimensional beam scanning based on the optimization of array geometry," *Electromagnetics*, vol. 32, no. 6, pp. 305–320, Aug, 2012.

[11] L. Zhang, Y.-C. Jiao, B. Chen, and Z.-B. Weng. "Multiobjective optimization design of concentric ring arrays with 3D beam scanning using differential evolution algorithm," *Int. J. Numer. Model. Electron. Netw. Devices Fields*, vol. 26, no. 6, pp. 602–619, Sep, 2012.

[12] W. Liang, Z. Wu, and L. Zhang, "Multiobjective optimization design of time-modulated concentric circular ring arrays," *Int. J. Antenn. Propag.*, vol. 2018, Mar. 2018, Art. no. 6056139.

[13] P. Ioannides and C. A. Balanis, "Uniform circular and rectangular arrays for adaptive beamforming applications," *IEEE Antennas Wireless Propag. Lett.*, vol. 4, pp. 351–354, 2005.

[14] M. G. M. Hussain, "Beamforming with uniform-circular-array and ultrawideband-throb signal," in *Proc. IEEE Int. Symp. Phased Array Syst. Technol. (PAST)*, Waltham, MA, USA, 2022, pp. 1–8.

[15] V. Zuniga, N. Haridas, A. T. Erdogan, and T. Arslan, "Effect of a central antenna element on the directivity, half-power beamwidth and side-lobe level of circular antenna arrays," in *Proc. NASA/ESA Conf. Adapt. Hardw. Syst.*, San Francisco, CA, USA, 2009, pp. 252–256.

[16] T. B. Vu, "Side-lobe control in circular ring array," *IEEE Trans. Antennas Propag.*, vol. 41, no. 8, pp. 1143–1145, Aug. 1993.

[17] R. Vescovo, "Constrained and unconstrained synthesis of array factor for circular arrays," *IEEE Trans. Antennas Propag.*, vol. 43, no. 12, pp. 1405–1410, Dec. 1995.

[18] B. K. Lau and Y. H. Leung, "A Dolph-Chebyshev approach to the synthesis of array patterns for uniform circular arrays," in *Proc. IEEE Int. Symp. Circuits Syst. (ISCAS)*, vol. 1, Geneva, Switzerland, 2000, pp. 124–127.

[19] S. C. Chan and C. K. S. Pun, "On the design of digital broadband beamformer for uniform circular array with frequency invariant characteristics," *Proc. IEEE Int. Symp. Circuits Syst.*, Phoenix-Scottsdale, AZ, USA, 2002, pp. 693–696.

[20] L. Biller and G. Friedman, "Optimization of radiation patterns for an array of concentric ring sources," *IEEE Trans. Audio Electroacoust.*, vol. 21, no. 1, pp. 57–61, Feb. 1973.

[21] D. Huebner, "Design and optimization of small concentric ring arrays," in *Proc. Antennas and Propag. Soc. Int. Symp.*, Washington, DC, USA, 1978, pp. 455–458.

[22] B. P. Kumar and G. R. Branner, "Design of low sidelobe circular ring arrays by element radius optimization," *Proc. IEEE Antennas Propag. Soc. Int. Symp.*, Orlando, FL, USA, 1999, pp. 2032–2035 vol. 3.

[23] C. Stearns and A. Stewart, "An investigation of concentric ring antennas with low sidelobes," *IEEE Trans. Antennas Propag.*, vol. 13, no. 6, pp. 856–863, Nov. 1965.

[24] H. J. Visser. *Array and Phased Array Antenna Basics*. Hoboken, NJ, USA: Wiley, 2006.

[25] R. J. Mailloux, *Phased Array Antenna Handbook*. Norwood, MA, USA: Artech House, 2017.

[26] P. Nayeri, F. Yang, and A. Z. Elsherbeni, "Beam-scanning reflectarray antennas: A technical overview and state of the art," *IEEE Antennas Propag. Mag.*, vol. 57, no. 4, pp. 32–47, Aug. 2015.

[27] N. H. Noordin, V. Zuniga, A. O. El-Rayis, N. Haridas, A. T. Erdogan, and T. Arslan, "Uniform circular arrays for phased array antenna," in *Proc. Loughborough Antennas Propag. Conf.*, Loughborough, U.K., 2011, pp. 1–4.

[28] M. A. Panduro, C. A. Brizuela, L. I. Balderas, and D. A. Acosta, "A comparison of genetic algorithms, particle swarm optimization and the differential evolution method for the design of scannable circular antenna arrays," *Prog. Electromagn. Res. B*, vol. 13, pp. 171–186, Jan. 2009.

[29] P. Ghosh and S. Das. "Synthesis of thinned planar concentric circular antenna arrays–A differential evolutionary approach," *Progr. Electromagn. Res. B*, vol. 29, pp. 63–82, Jan. 2011.

[30] K. V. Price, "Differential evolution," in *Handbook of Optimization*. Berlin, Germany: Springer, 2013, pp. 187–214.

[31] Y. Ya-Li, F. Guang, G. Shu-Xi, C. Xi. and L. Dong-Chao, "Design of a wide-band Yagi-Uda antenna using differential evolution algorithm," in *Proc. Int. Symp. Signals Syst. Electron.*, Nanjing, China, 2010, pp. 1–4.

[32] S. Yang, Y. B. Gan, and A. Qing, "Sideband suppression in time-modulated linear arrays by the differential evolution algorithm," *IEEE Antennas Wireless Propag. Lett.*, vol. 1, pp. 173–175, 2002.

[33] N. Dib, S. Goudos, and H. Muhsen, "Application of Taguchi's optimization method and self-adaptive differential evolution to the synthesis of linear antenna arrays," *Prog. Electromagn. Res.*, vol. 102, pp. 159–180, Jan. 2010.

[34] D. G. Kurup, M. Himdi, and A. Rydberg, "Synthesis of uniform amplitude unequally spaced antenna arrays using the differential evolution algorithm," *IEEE Trans. Antennas Propag.*, vol. 51, no. 9, pp. 2210–2217, Sep. 2003.

[35] A. F. Morabito, A. Di Carlo, L. Di Donato, T. Isernia, and G. Sorbello, "Extending spectral factorization to array pattern synthesis including sparseness, mutual coupling, and mounting-platform effects," *IEEE Trans. Antennas Propag.*, vol. 67, no. 7, pp. 4548–4559, Jul. 2019.